Available online at www.sciencedirect.com

ScienceDirect

Mendeleev Commun., 2022, **32**, 132–135

Mendeleev Communications

Magnetic resonance tracking of copper ion fixation on the surface of carboxylated nanodiamonds from viewpoint of changes in carbon-inherited paramagnetism

Vladimir Yu. Osipov,*[a] Nikolai M. Romanov,[b,c] Inna E. Suvorkova,[d] Ekaterina V. Osipova,[e] Takuma Tsuji,[f] Yasushi Ishiguro[g] and Kazuyuki Takai[f]

[a] *Ioffe Institute, Russian Academy of Sciences, 194021 St. Petersburg, Russian Federation. Fax: +7 812 297 1017; e-mail: osipov@mail.ioffe.ru*
[b] *School of Engineering Science, LUT University, 53850 Lappeenranta, Finland*
[c] *Joint-Stock Company 'Svetlana-Semiconductors', 194156 St. Petersburg, Russian Federation*
[d] *Institute of Chemistry, Saint Petersburg State University, 198504 Petergof, St. Petersburg, Russian Federation*
[e] *Saint Petersburg State Institute of Technology, 190013 St. Petersburg, Russian Federation*
[f] *Department of Chemical Science and Technology, Hosei University, Koganei, 184-8584 Tokyo, Japan*
[g] *Department of Electrical and Electronic Engineering, Tokyo Denki University, 120-8551 Tokyo, Japan*

DOI: 10.1016/j.mencom.2022.01.043

Detonation nanodiamonds with a particle size of 5 nm and a carboxylated surface are easily modified by doubly charged copper ions to form copper chelate complexes. The concentration of copper complexes in a dry powder of such nanodiamonds is well monitored by the method of electron paramagnetic resonance, both by the signal width of intrinsic paramagnetic centers in nanodiamonds and by the signal shape for the surface Cu^{2+} ions themselves, including the set of hyperfine splitting lines for the parallel component and the line with an unresolved hyperfine structure for the perpendicular component.

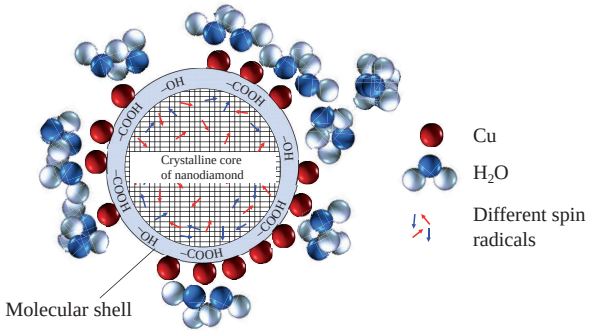

Keywords: detonation nanodiamond, copper ions, chelate complexes, surface functional groups, spin paramagnetism, elemental analysis, electron paramagnetic resonance.

Detonation diamonds (DND) with a particle size of 5 nm are among the most attractive modern nanoscale precursors on the global market.[1–4] They occupy an intermediate position between a solid and polymer-type biomolecules with a moderately high molecular weight below 150 000. The surface of commercially available DNDs is mainly saturated with oxygen-containing groups, but it is easy to functionalize with other groups and atoms, which are well diagnosed by various methods.[5–8] The surface of such diamonds can be carboxylated,[9,10] which opens the way for the production of various DND derivatives based on chelation of 3*d* and 4*f* metal ions with surface groups and their subsequent complex transformations.[11–13]

The method of copper ion chelation on the DND surface in an aqueous suspension has already been published, and the electron paramagnetic resonance (EPR) study of the resulting dry product revealed two types of EPR signals: signals from dangling bonds in the carbon matrix and signals from copper ions with the $3d^9$ configuration.[14–16] Based on these previously obtained EPR data, the depth of the location of the main paramagnetic centers in DND particles was determined.[17]

Nevertheless, the process of fixing copper and other metal ions on the surface of carboxylated 5-nm DND particles from various commercial manufacturers has not been studied, and the question of the method reproducibility, together with the influence of third uncontrolled technological factors, remained open for a long time. In this work, we have successfully solved this problem and demonstrated the possibility of chelating copper ions at a concentration of up to 1.6–2 wt% on the surface of commercial carboxylated DNDs. It is shown that the EPR method[18,19] can distinguish signals from two types of spins: the carbon spins proper, localized inside DND particles, and the spins of doubly charged copper ions on the surface. We carried out this work on 5-nm DND from an aqueous suspension of single particles with a negative zeta potential (Adamas Nanotechnologies).

The fixation of copper on the surface of DND particles using chelation was carried out by the method described in Online Supplementary Materials. When obtaining samples designated D1, D2 and D3, the volumes and concentrations of saline solutions were selected so that during the chelation reaction in the mixture, nominally 1, 2.5 and 5 wt% of copper atoms were adsorbed on DND particles, respectively, assuming 100% sorption efficiency. Here, the original dried precursor powder isolated from the aqueous DND suspension obtained from the manufacturer was designated as DND-ini, and labels D1–D3 denote the above dried copper-modified products made according to the scheme outlined in Figure S2 (see Online Supplementary Materials). The actual concentration of chelated copper found in D1 was in line with technological expectations, while for D2 and D3, as will be seen later, it was about 1.9 and 3 times lower than the predicted calculated one.

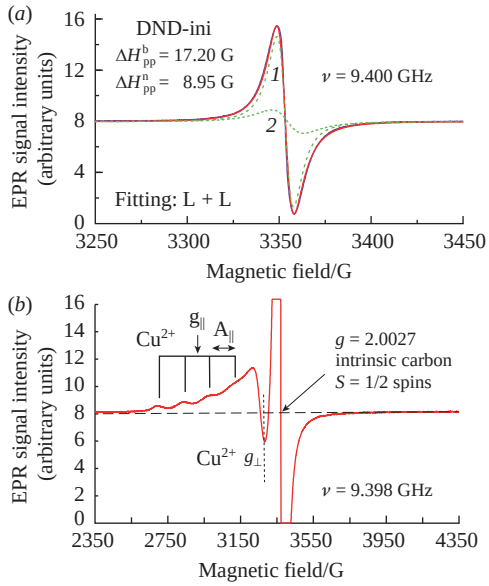

Figure 1 EPR spectra of samples (*a*) DND-ini and (*b*) D2 obtained in different ranges of magnetic fields for (*a*) the intrinsic paramagnetic spins $S = 1/2$ in sample DND-ini and (*b*) for the Cu^{2+} spins in sample D2 with parallel (demonstrating a pronounced hyperfine structure) and perpendicular components, as well as for the intrinsic spins of the DND matrix. Measurement conditions: microwave power of 2 mW, magnetic field modulation amplitude of 1.2 G and $T = 293$ K. (*a*) The EPR singlet signal of sample DND-ini consists of (*1*) narrow and (*2*) broad Lorentzian components.

The EPR spectra of samples DND-ini and D2 are shown in Figure 1 in different representations. One of them uses a narrow range of magnetic fields with a width of 200 G [Figure 1(*a*)] to display the main EPR signal of sample DND-ini ($g = 2.0027$) caused by dangling covalent bonds in the diamond lattice or unpaired spins of another origin. The other covers an interval 2000 G wide, including the low- and high-field spectral regions [Figure 1(*b*)], to represent the EPR signal of Cu^{2+} ions in sample D2 with a well-resolved hyperfine structure of the signal from the parallel component $g = g_{\|}$ and an unresolved structure from the perpendicular component $g = g_{\perp}$ against the background of a central high-intensity signal from the DND spins. The spectrum in Figure 1(*b*) contains a well-recognized hyperfine structure from Cu^{2+} ions for the parallel signal component with $g = g_{\|}$ (in the range of 2350–3150 G) and the low-field wing of the Cu^{2+} line for the perpendicular component (in the range below 3250 G). In this case, the high-field wing of this line $g = g_{\perp}$ (above 3250 G) is hardly distinguishable and strongly overlaps with the intense EPR signal ($g = 2.0027$) from the DND carbon matrix.† The latter is centered at ~3353 G (the magnetic field is corrected) and has a linewidth ΔH_{pp} of about 12.4 G (the distance between the peaks in the spectrum of the first derivative of the microwave absorption signal). Note that the ΔH_{pp} value ($g = 2.0027$) for sample DND-ini (no copper ions) is ~9.2 G. It is approximately ~1 G higher than the previously measured ΔH_{pp} values for DNDs, well purified from 3*d* metals, in aggregated or disaggregated forms. As can be seen from Figure 1(*a*), the EPR singlet signal from the carbon matrix consists of two superimposed Lorentz-shaped components, narrow (L1) and broad (L2).‡ The presence of a broad component (line) follows from the impossibility of describing the singlet signal by a single Lorentzian contour with a small width at half maximum. It was previously found[17] that both of these components of the EPR signal can be attributed to shallow (<1.1 nm) and deep (>1.1 nm) paramagnetic defects under the surface of diamond particles, which are relatively stable and well protected from direct reactions and exchange with other spin radicals from the external atmosphere. In this case, the broad Lorentzian component [see Figure 1(*a*), curve *2*] corresponds to conventionally shallow paramagnetic centers. The outer layer, 0.8 nm thick, enriched with paramagnetic defects, is to a certain extent caused by a slight structural disordering of the diamond lattice in the regions adjacent to the outer boundary, so that, in general, the tetrahedral coordination for carbon atoms is retained. As previously shown[20] by NMR spectroscopy, the thickness of this disordered layer is about 0.6 nm. It also contains a predominant amount of nitrogen atoms in the form of zero-spin diamagnetic nitrogen pairs NN.[21,22]

The EPR spectrum of sample D2 shown in Figure 1(*b*) is presented in Figure 2(*a*) in integral representation.§ Such an integrated spectrum rather well resolves the EPR signals from ½ spins of both types ('carbon' and 'copper') in a wide range of magnetic fields and makes it possible to compare them quantitatively. The decomposition of the integrated EPR spectrum into components from the copper and carbon subsystems is described in Online Supplementary Materials. The inset in Figure 2(*a*) shows, for example, the EPR signal only from Cu^{2+} ions in sample D2 in the integral representation. In this inset, the spectrum features are assigned to the $g_{\perp}$ and $g_{\|}$ components of the Cu^{2+} signal. In the D1–D3 series, a 1.48-fold increase in the integrated intensity of the EPR signal from Cu^{2+} and, consequently, the actual content of ionic copper is observed. In this case, the integrated intensity of the EPR signal ($g = 2.0027$) from paramagnetic defects in the

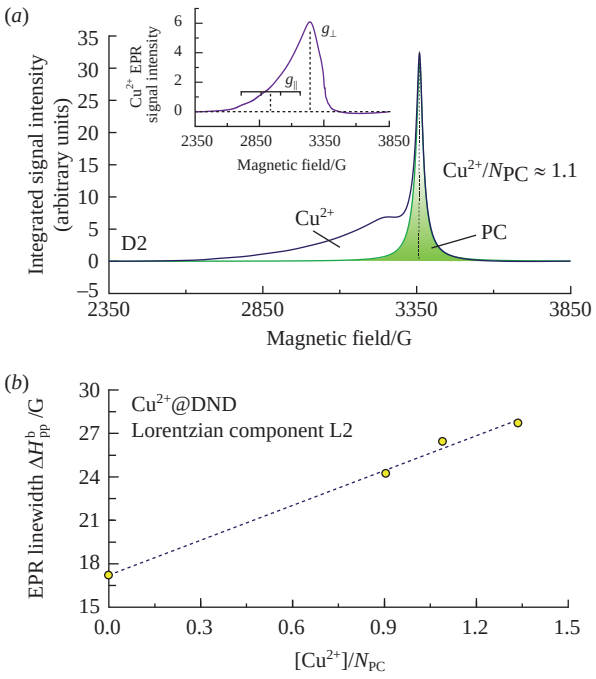

Figure 2 (*a*) Integrated EPR spectrum of sample D2 obtained by integration over the variable magnetic field (H) in the range of 2350–3850 G. The inset demonstrates the integrated EPR spectrum of Cu^{2+} ions in sample D2 obtained by subtracting the DND spectrum. Similar EPR curves for other samples are shown in Figure S3. (*b*) The dependence of the width of the Lorentzian component L2 of the DND spectrum (shaded in green) on the Cu^{2+} concentration. Measurement conditions: $T = 293$ K, microwave frequency is 9.397 ± 0.001 GHz.

† For this reason, in previously published works, the perpendicular component of the Cu^{2+} EPR signal was not investigated and was not taken into account when assessing the content of ionic copper.

‡ As suggested earlier,[17] this procedure of decomposing the central line into two components was performed for the EPR spectra of all series samples.

§ The experimentally measured EPR spectrum is the spectrum of the first derivative of microwave absorption with respect to the magnetic field (dA/dH). Its recording is carried out by an analog method by modulating a constant magnetic field (H_o) with a weak alternating field ($H^{\sim}$) at a frequency of 100 kHz with a modulation amplitude of up to 3 G.

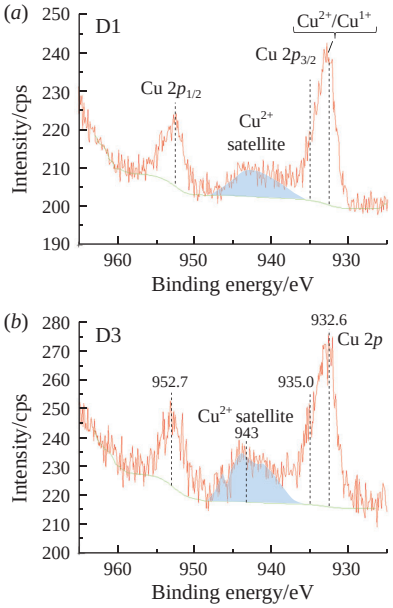

Figure 3 Fragments of XPS spectra of samples (*a*) D1 and (*b*) D3 for the peaks Cu $2p_{1/2}$ and Cu $2p_{3/2}$, separated by the spin-orbit splitting of the 2*p* level by ~20 eV.

diamond matrix remains practically unchanged. But the signal width changes by 30–40%. This increase in copper content is also confirmed by the SEM-EDX¶ data, which for the D1–D3 series samples give N_{Cu} values of 0.99, 1.34 and 1.65 wt%, respectively. With an increase in the Cu^{2+} concentration, the broad (L2) and narrow (L1) components of the EPR signal of DND broaden due to the dipole–dipole mechanism[23,24] of interaction between ½ spins of different types located both inside a 5 nm particle and on its surface in the form of Cu^{2+} ions [Figure 2(*b*) and Online Supplementary Materials]. This broadening indicates the fixation of ionic copper near (within 0.3 nm) of the DND surface. The dependences of both narrow and broad line widths (ΔH^{n}_{pp} and ΔH^{b}_{pp}, respectively) on Cu^{2+} content (Figure S5) show features different from those previously reported.[17] The latter is due to both the large actual values of N_{Cu} (more than 0.99 wt%) and $[Cu^{2+}]/N_{PC}$ and the use of DND precursor in the form of a suspension of single 5-nm particles, rather than 30–35 nm aggregates based on them. Another feature of this precursor is the presence of traces of foreign metal impurities.

Difference EPR signals related to Cu^{2+} ions were calculated for all D1–D3 series samples with normalization to the total number of spin radicals in the diamond matrix (Figure S4). Both in a wide range of magnetic fields and in specific details, the shape of all these EPR signals turned out to be approximately unchanged and the same as in the inset in Figure 2(*a*). This similarity indicates that for different concentrations of chelated copper of more than 1 wt%, one type of copper chelate complexes is formed on the DND surface and characterized by the identical parameters of the spin Hamiltonian.[18] Moreover, the EPR signal of Cu^{2+} ions is characterized by such parameters as $g_{\perp} = 2.0748$, $g_{||} = 2.322$ and $A_{||} = 144$ G. A value of 1.6 wt% corresponds to the practical sorption limit†† of the entire active surface of particles, above which the use of the aqueous method for further chemical adsorption of copper becomes difficult.

The presence of copper ions on the DND surface was also confirmed by X-ray photoelectron spectroscopy (XPS).‡‡,[25,26] This method, designed to analyze the composition and types of bonds between elements, was previously used to study the DND surface.[27–29] Both survey XPS spectra of all samples in the range from 0 to 1350 eV and detailed spectra of C 1*s*, N 1*s*, Zr 3*d* and Cu 2*p* peaks for samples D1 and D3 were recorded. The spectra of Cu 2*p* signals are shown in Figures 3(*a*),(*b*) for samples D1 and D3 with the most strongly differing copper concentrations. For both samples, the spectra of the Cu 2*p* peaks are approximately similar. Sample D3 shows a well-defined Cu 2*p* signal with three lines at ~932.6, ~943 and ~952.7 eV [Figure 3(*b*)]. The components $2p_{1/2}$ (952.7 eV) and $2p_{3/2}$ (932.6 eV) of the Cu 2*p* peak are determined by the spin-orbit splitting of the Cu 2*p* level ($\Delta \approx 19.8$ eV),[30] and the intensity ratio of the components is ~1/2. Each of the components $2p_{1/2}$ and $2p_{3/2}$ is due to copper in the charge state Cu^{1+} and Cu^{2+} and, in turn, can be decomposed into two strongly overlapping bands. This is clearly seen for the $2p_{3/2}$ peak of sample D3 [see Figure 3(*b*)]. The peak (central band) at ~943 eV is satellite and is mainly due to copper in the Cu^{2+} state. The integrated intensity of the band at ~943 eV is higher in sample D3 than in sample D1, which indicates a larger fraction of copper atoms in the Cu^{2+} state in it. The integrated intensities of Cu 2*p* signals in samples D1 and D3 correspond to the copper content of 1.42 and 2.28 wt%, respectively. These values are about 1.4 times higher than the values (0.99 and 1.65 wt%) obtained by the SEM-EDX method. For samples D1 and D3, the Cu/C atomic ratios are 0.0034 and 0.0056, and the weight contents of copper are 1.48 and 2.38 wt%, respectively. These values correspond to ~39 and ~64 copper atoms on the surface of a 5-nm DND particle, consisting of 11 500 carbon atoms. At the same time, for sample D3, the O/C ratio is 0.148, which corresponds to approximately 1700 oxygen atoms on the surface of a 5-nm DND particle. To a rough approximation that all oxygen is concentrated in carboxyl groups, this means that for sample D3 with the maximum realized copper content, only ~15% of all pairs of carboxyl groups are bound to copper atoms while the rest of the pairs are not involved. It is noteworthy that the XPS method detects about two and a half times more copper atoms on the DND surface than the paramagnetic ½ spins attributed to the Cu^{2+} ions (see Online Supplementary Materials). Some copper may be on the surface in states other than Cu^{2+}, such as Cu^{1+} or clusters of several atoms. The criterion for the correctness of the performed studies is that the content of impurity nitrogen in the inner regions of DND particles in all samples is ~2.3 at%, which entirely agrees with the known data[21] and does not depend on the process of chemical adsorption of copper atoms by particles.

The data obtained by EPR, EDX and XPS methods are generally in good agreement with each other, considering that, at a copper content of more than 1 wt%, some of it can be found on the DND surface in forms other than Cu^{2+}.

Thus, for concentrations of chelated copper on the surface of DND particles above 1 wt%, express tracking of the approximate copper content can be performed by recording the broadening of the main DND EPR signal, including its narrow (>9 G) and broad (>17 G) Lorentz-type components. This procedure does not require weighing the sample to be measured. In turn, the quantitative analysis of copper in the Cu^{2+} state can be carried out by double integration of the EPR signal of the Cu^{2+}@DND sample in a wide range of magnetic fields (±1000 G) with the subsequent subtraction from it of the contribution from the DND intrinsic paramagnetic centers (singlet signal with a *g*-factor of 2.0027). An additional independent calibration can be the concentration of paramagnetic centers in DND (~1300 ppm or ~15 spins per 5-nm particle), which is approximately the same (in a confidence interval of ±25%) for all commercially available DNDs produced

¶ SEM-EDX is an energy-dispersive X-ray spectroscopy (EDX) unit implemented as a built-in analyzer in a scanning electron microscope (SEM).
†† According to XPS spectroscopy, which provides information from a depth of no more than 10 nm, this limit is slightly higher – 2.6 wt%.
‡‡ The complex XPS spectrometer of the St. Petersburg State University was used.

from the optimal (in terms of product yield[4]) mixture of trinitrotoluene–hexogen. This approach is, in principle, applicable to other Cu-DND structures obtained by alternative methods.[31]

In conclusion, the amount of ionic copper on the surface of DND particles in the concentration range above 1 wt% can be estimated by recording the broadening of the main EPR signal of DND, including its broader (>17 G) Lorentzian component associated with shallow paramagnetic centers.

V.O. thanks the Russian Foundation for Basic Research (project no. 18-29-19038 MK). K.T. acknowledges the support of JSPS KAKENHI (grant nos. 19K05410 and 26107532). I.S. thanks the Research Park of Saint-Petersburg State University for help in carrying out measurements. E.O. is grateful to Hosei University for providing the equipment for the synthesis.

Online Supplementary Materials

Supplementary data associated with this article can be found in the online version at doi: 10.1016/j.mencom.2022.01.043.

References

1 *Detonation Nanodiamonds: Science and Applications*, eds. A. Ya. Vul' and O. A. Shenderova, Pan Stanford, Singapore, 2014.
2 *Nanodiamonds: Advanced Material Analysis, Properties and Applications*, ed. J.-C. Arnault, Elsevier, Amsterdam, 2017.
3 A. Krueger, in *Nanodiamond (Nanoscience series)*, ed. O. A. Williams, Royal Society of Chemistry, Cambridge, 2014, pp. 49–88.
4 V. Yu. Dolmatov, A. N. Ozerin, I. I. Kulakova, O. O. Bochechka, N. M. Lapchuk, V. Myllymäki and A. Vehanen, *Russ. Chem. Rev.*, 2020, **89**, 1428.
5 M. Dubois, K. Guérin, N. Batisse, E. Petit, A. Hamwi, N. Komatsu, H. Kharbache, P. Pirotte and F. Masin, *Solid State Nucl. Magn. Reson.*, 2011, **40**, 144.
6 M. Dubois, K. Guérin, E. Petit, N. Batisse, A. Hamwi, N. Komatsu, J. Giraudet, P. Pirotte and F. Masin, *J. Phys. Chem. C*, 2009, **113**, 10371.
7 C. Presti, A. S. Lilly Thankamony, J. G. Alauzun, P. H. Mutin, D. Carnevale, C. Lion, H. Vezin, D. Laurencin and O. Lafon, *J. Phys. Chem. C*, 2015, **119**, 12408.
8 V. Yu. Osipov, N. M. Romanov, K. Kogane, H. Touhara, Y. Hattori and K. Takai, *Mendeleev Commun.*, 2020, **30**, 84.
9 V. Yu. Osipov, A. E. Aleksenskiy, A. I. Shames, A. M. Panich, M. S. Shestakov and A. Ya. Vul', *Diamond Relat. Mater.*, 2011, **20**, 1234.
10 D. G. Lim, K. H. Kim, E. Kang, S. H. Lim, J. Ricci, S. K. Sung, M. T. Kwon and S. H. Jeong, *Int. J. Nanomed.*, 2016, **11**, 2381.
11 V. Yu. Osipov, D. W. Boukhvalov and K. Takai, *Mendeleev Commun.*, 2020, **30**, 436.
12 A. M. Panich, A. I. Shames, N. A. Sergeev, V. Yu. Osipov, A. E. Alexenskiy and A. Ya. Vul', *J. Phys. Chem. C*, 2016, **120**, 19804.
13 K. Yano, T. Matsumoto, Y. Okamoto, K. Bito, N. Kurokawa, T. Hasebe and A. Hotta, *ACS Appl. Nano Mater.*, 2021, **4**, 1702.
14 I. D. Gridnev, V. Yu. Osipov, A. E. Aleksenskii, A. Ya. Vul' and T. Enoki, *Bull. Chem. Soc. Jpn.*, 2014, **87**, 693.
15 A. I. Shames, A. M. Panich, V. Yu. Osipov, A. E. Aleksenskiy, A. Ya. Vul', T. Enoki and K. Takai, *J. Appl. Phys.*, 2010, **107**, 014318.
16 V. Yu. Osipov, D. W. Boukhvalov and K. Takai, *Mendeleev Commun.*, 2019, **29**, 452.
17 A. I. Shames, V. Yu. Osipov, A. E. Aleksenskiy, E. Ōsawa and A. Ya. Vul', *Diamond Relat. Mater.*, 2011, **20**, 318.
18 J. E. Wertz and J. R. Bolton, *Electron Spin Resonance: Elementary Theory and Practical Applications*, McGraw-Hill, New York, 1972.
19 A. Lund, M. Shiotani and S. Shimada, *Principles and Applications of ESR Spectroscopy*, Springer, Dordrecht, 2011.
20 X. Fang, J. Mao, E. M. Levin and K. Schmidt-Rohr, *J. Am. Chem. Soc.*, 2009, **131**, 1426.
21 S. Turner, O. Shenderova, F. Da Pieve, Y. Lu, E. Yücelen, J. Verbeeck, D. Lamoen and G. Van Tendeloo, *Phys. Status Solidi A*, 2013, **210**, 1976.
22 I. A. Dobrinets, V. G. Vins and A. M. Zaitsev, *HPHT-Treated Diamonds: Diamonds Forever*, Springer, Berlin, 2013.
23 N. Kobayashi, T. Enoki, C. Ishii, K. Kaneko and M. Endo, *J. Chem. Phys.*, 1998, **109**, 1983.
24 C. P. Slichter, *Principles of Magnetic Resonance*, Harper & Row, New York, 1963.
25 J. F. Moulder, W. F. Stickle, P. E. Sobol and K. D. Bomben, *Handbook of X-ray Photoelectron Spectroscopy*, ed. J. Chastain, Perkin-Elmer Corp., Eden Prairie, MN, 1992.
26 P. van der Heide, *X-ray Photoelectron Spectroscopy: An Introduction to Principles and Practices*, John Wiley & Sons, Hoboken, NJ, 2011.
27 A. E. Aleksenskii, V. Yu. Osipov, A. Ya. Vul', B. Ya. Ber, A. B. Smirnov, V. G. Melekhin, G. J. Adriaenssens and K. Iakoubovskii, *Phys. Solid State*, 2001, **43**, 145 (*Fiz. Tverd. Tela*, 2001, **43**, 140).
28 J. C. Arnault, *Diamond Relat. Mater.*, 2018, **84**, 157.
29 E.-Z. Piña-Salazar, R. Kukobat, R. Futamura, T. Hayashi, S. Toshio, E. Ōsawa and K. Kaneko, *Carbon*, 2018, **139**, 853.
30 D. C. Frost, A. Ishitani and C. A. McDowell, *Mol. Phys.*, 1972, **24**, 861.
31 K. Turcheniuk and V. N. Mochalin, *Carbon*, 2016, **109**, 98.

Received: 14th July 2021; Com. 21/6613